Weierstraß-Institut
für Angewandte Analysis und Stochastik

im Forschungsverbund Berlin e.V.

Preprint ISSN 0946 – 8633

Quantifying hydrodynamic slip: A comprehensive analysis of dewetting profiles

R. Fetzer[1], A. Münch[2], B. Wagner[3], M. Rauscher[4] K. Jacoobs[5]

submitted: April 18, 2007

[1] Saarland University, Department of Experimental Physics, D-66123 Saarbrücken, Present address: University of South Australia, Ian Wark Research Institute, Mawson Lakes, SA 5095, Australia

[2] Humboldt University of Berlin, Institute of Mathematics, D-10099 Berlin and Weierstrass Institute for Applied Analysis and Stochastics (WIAS), Mohrenstraße 39, D-10117 Berlin

[3] Weierstrass Institute for Applied Analysis and Stochastics (WIAS), Mohrenstraße 39, D-10117 Berlin

[4] Max-Planck-Institute for Metals Research, Heisenbergstraße 3, D-70569 Stuttgart and University of Stuttgart, Institute for Theoretical and Applied Physics, Pfaffenwaldring 57, D-70569 Stuttgart

[5] Saarland University, Department of Experimental Physics, D-66123 Saarbrücken

No. 1220

Berlin 2007

2000 *Mathematics Subject Classification.* 76D08 76E17 74A55.

Key words and phrases. Polymer melts, slip boundary effects, interfacial and free surface flows, lubrication models, Stokes model.

Edited by
Weierstraß-Institut für Angewandte Analysis und Stochastik (WIAS)
Mohrenstraße 39
10117 Berlin
Germany

Fax: + 49 30 2044975
E-Mail: preprint@wias-berlin.de
World Wide Web: http://www.wias-berlin.de/

Abstract

To characterize non-trivial boundary conditions of a liquid flowing past a solid, the slip length is commonly used as a measure. From the profile of a retracting liquid front as measured, e.g., with atomic force microscopy, the slip length as well as the capillary number can be extracted by the help of the Stokes model for a thin liquid film dewetting from a solid substrate. Specifically, we use a lubrication model derived from the Stokes model for strong slippage and linearize the film profile around the flat, unperturbed film, and, for small slip lengths a Taylor approximation of the linearisation for the full Stokes model. Furthermore, from the capillary number and the knowledge of the liquid front velocity and the surface tension, we can obtain the viscosity of the fluid film. We compare theoretical and experimental results, test the consistency and the validity of the models/approximations, and give an easy-to-follow manual of how they can be used to analyze experiments.

1 Introduction

In microfluidic devices, the drag of a fluid is a substantial concern since, for a given pumping power, it limits the microfluidic channel length that can be filled. It therefore sets also the limits to, e.g., the number of possible analysis steps. Drag can be reduced by decreasing the friction at the liquid/solid interface or, in other words, by increasing the fluid velocity at the interface. This results in a sliding of the fluid over the solid, and a non-zero boundary condition for the interface velocity. The amount of slippage is typically characterized by the depth b below the solid-liquid interface at which the extrapolated velocity vanishes.

To date, a number of methods exist to determine the slip length, most of them involving tracer particles [1, 2], fluorescence recovery after photobleaching [3, 4], colloidal probe microscopy [5, 6], or surface forces apparatus [7, 8]. Detailed reviews can be found in recent articles by Lauga et al. [9] or Neto et al. [10]. In our previous studies [11, 12, 13], we have introduced a new method to gain interfacial flow properties, namely the analysis of the profile of a liquid front. Specifically, we exploit that the amount of slippage has a significant influence on the decay of the profile onto the unperturbed films, where the model equations can be linearized. A more comprehensive asymptotic analysis of the entire profile in the presence of large slippage, which necessarily must consider all nonlinearities, is a separate direction of (in part still ongoing) research [14]. For the purpose here, the information obtained from the linearized model(s) is sufficient to obtain the slip length by fitting the eigenvalues that govern the decay of the profile to the experimentally measured film profiles. The method works well for viscous fluids dewetting from a solid surface and is based on a lubrication model with a Navier-slip condition for the flow of a Newtonian liquid in the limit of strong effective slippage (large slip lengths).

To test this model, we also discuss here the full two dimensional description using the underlying Stokes model. We find that, while the strong slip lubrication model is valid in most of the interesting parameter regimes, i.e. where changes in the slippage have a significant impact on the film profile, the validity can be extended to smaller slip lengths by using a third order Taylor expansion for the eigenvalue relation characterizing the linearized film profile. The third order Taylor expansion of the Stokes model is able to extract slip length and capillary number quite accurately from experiments of dewetting fluids where the form of the profile is accessible, e.g., by atomic force microscopy (AFM). Via the capillary number, the viscosity can be gained if the dewetting velocity and the surface tension are known. In the following we will develop the theoretical approach, compare numerical and experimental results, introduce the Stokes model and its approximations, test their validity in many aspects, and give a recipe how they can be used to analyze experiments.

2 Formulation

Recently we have shown that the dewetting process of highly viscous polystyrene (PS) melts on hydrophobized silicon wafers is well described by a lubrication model in the regime of large slip lengths, [11, 13]. For the situation considered here, the flow is very slow and non-Newtonian properties, such as viscoelasticity of the melt, can be neglected. For the same reason, inertial terms will not play any role. For clarity of presentation and as in our previous studies, we will consider the effectively two dimensional situation of a liquid ridge, which is translationally invariant in the Y-direction parallel to the flat and homogeneous substrate. Hence, we begin our theoretical discussion with the Stokes equations for an incompressible fluid layer on $0 \leq Z \leq H(X,T)$ in two dimensions

$$-\nabla P + \eta\, \nabla^2 \mathbf{U} = 0, \qquad \nabla \cdot \mathbf{U} = 0, \tag{1}$$

together with appropriate boundary conditions (see below). Here, $\mathbf{U} = U(X,Z,T)\,\hat{\mathbf{e}}_{\mathbf{x}} + W(X,Z,T)\,\hat{\mathbf{e}}_{\mathbf{z}}$ denotes the velocity field, η the viscosity, and $P = P(X,Z,T)$ the pressure field.

At the free surface $Z = H(X,T)$, we have the usual kinematic condition for nonvolative fluids

$$\partial_T H = -\partial_X \int_0^H U(X,Z)dZ \tag{2}$$

and normal and tangential stress boundary conditions with constant surface tension σ

$$\boldsymbol{n} \cdot \boldsymbol{\tau} \cdot \boldsymbol{n} - (P - \Phi'(H)) = 2\,\sigma\,\kappa, \quad \text{and} \quad \boldsymbol{n} \cdot \boldsymbol{\tau} \cdot \boldsymbol{t} = 0, \tag{3}$$

with the stress tensor

$$\boldsymbol{\tau} = \eta \left[\nabla \mathbf{U} + \left(\nabla \mathbf{U}\right)^T\right], \tag{4}$$

and where $\Phi'(H) = d\Phi/dH$ denotes the contribution due to the effective interface potential $\Phi(H)$ (of Born/Van der Waals type), see e.g. [15] for details of the potential. The normal and tangential unit vectors are given by

$$\boldsymbol{n} = \frac{(-\partial_X H, 1)}{\sqrt{1 + (\partial_X H)^2}} \quad \text{and} \quad \boldsymbol{t} = \frac{(1, \partial_X H)}{\sqrt{1 + (\partial_X H)^2}}, \tag{5}$$

where the local mean curvature is $\kappa = \nabla \cdot \boldsymbol{n}$. At $Z = 0$, we assume impermeability of the substrate and the Navier-slip boundary condition,

$$W = 0 \quad \text{and} \quad U = B\,\partial_Z U, \tag{6}$$

with the Navier slip length B.

We non-dimensionalize the above system of equations using the following scales

$$\begin{array}{lllllllllll} Z &=& \bar{H}\,z, & X &=& \bar{L}\,x, & H &=& \bar{H}\,h, & B &=& \bar{H}\,b, \\ U &=& \bar{U}\,u, & W &=& \bar{W}\,w, & T &=& \frac{\bar{H}}{\bar{W}}t, & P &=& \bar{P}\,p, \\ \Phi' &=& \bar{P}\,\phi'. \end{array} \tag{7}$$

The vertical length scale $\bar{H}$ is fixed by the average film thickness and the lateral length scale $\bar{L}$ by the competition of the effective interface potential and the surface tension, i.e., by the dispersive capillary length. The vertical and horizontal velocity scale are linked via the incompressibility condition $\bar{U} = \bar{L}\,\bar{W}/\bar{H}$. The choice of the pressure scale $\bar{P}$ and of the velocity scale $\bar{U}$ together with the magnitude of b fixes the flow regime.

In [12] it is shown that also for large slip lengths, i.e., for $b \gg 1$, the scale separation $\bar{H}/\bar{L} = \varepsilon \ll 1$ allows for the derivation of a simplified lubrication model, where the flow field is essentially plug flow. This implies a balance of the pressure gradient with the dominant viscosity contribution in the vertical momentum equation, which yields the scaling

$$\frac{\bar{P}\,\bar{H}}{\eta\,\bar{U}} \sim \varepsilon.$$

We assume that surface tension and pressure balance in the normal stress condition (and therefore surface tension does play a role in the dynamics of the film), i.e.,

$$\frac{\sigma}{\bar{P}\,\bar{H}} \sim \varepsilon^{-2},$$

so that

$$\bar{U} = \frac{\sigma\,\varepsilon}{\eta} \quad \text{and} \quad \mathrm{Ca} = \frac{\eta\,\bar{U}}{\sigma} = \varepsilon. \tag{8}$$

In addition we assume $b = \beta/\varepsilon^2$ with $\beta = O(\varepsilon^0)$, i.e., that the slip length is large as compared to the lateral length scale $\bar{L}$. The non-dimensional problem in the *strong-slip* scaling is therefore

$$-\varepsilon^2\,\partial_x p + \varepsilon^2\,\partial_x^2 u + \partial_z^2 u = 0, \tag{9}$$

$$-\partial_z p + \varepsilon^2\,\partial_x^2 w + \partial_z^2 w = 0, \tag{10}$$

$$\partial_x u + \partial_z w = 0, \tag{11}$$

with boundary conditions at $z = h(x,t)$,

$$\begin{aligned} \partial_t h - w + u\,\partial_x h &= 0, && (12)\\ \left(\partial_z u + \varepsilon^2\,\partial_x w\right)\left(1 - \varepsilon^2\,(\partial_x h)^2\right) + 2\,\varepsilon^2\,\partial_x h\,\left(\partial_z w - \partial_x u\right) &= 0, && (13)\\ p - \phi'(h) - 2\,\frac{\left(1 - \varepsilon^2\,(\partial_x h)^2\right)\,\partial_z w - \partial_x h\,\left(\partial_z u + \varepsilon^2\,\partial_x w\right)}{1 + \varepsilon^2\,(\partial_x h)^2} & \\ + \frac{\partial_x^2 h}{\left(1 + \varepsilon^2\,(\partial_x h)^2\right)^{3/2}} &= 0, && (14) \end{aligned}$$

and boundary conditions at $z = 0$,

$$w = 0 \quad \text{and} \quad u = b\,\partial_z u = \frac{\beta}{\varepsilon^2}\,\partial_z u. \tag{15}$$

As shown in detail in [12], assuming that u, w, p and h have the asymptotic expansions

$$\begin{aligned} u(x,z,t;\varepsilon) &= u_0(x,z,t) + \varepsilon^2\,u_1(x,z,t) + O(\varepsilon^4), && (16)\\ w(x,z,t;\varepsilon) &= w_0(x,z,t) + \varepsilon^2\,w_1(x,z,t) + O(\varepsilon^4), && (17)\\ p(x,z,t;\varepsilon) &= p_0(x,z,t) + \varepsilon^2\,p_1(x,z,t) + O(\varepsilon^4), && (18)\\ h(x,t;\varepsilon) &= h_0(x,t) + \varepsilon^2\,h_1(x,t) + O(\varepsilon^4), && (19) \end{aligned}$$

and integrating the problem to $O(\varepsilon^2)$ the lubrication model for strong slip is found to be

$$\frac{4}{h_0}\,\partial_x(h_0\,\partial_x u_0) + \partial_x\left(\partial_x^2 h_0 - \phi'(h_0)\right) - \frac{u_0}{\beta\,h_0} = 0, \tag{20}$$

where the solution of the leading order problem implies that $u_0 = u_0(x,t)$. The first term on the left side is proportional to the divergence of the total longitudinal shear stress integrated over the film thickness. The second term is the gradient of the pressure in the film. This equation, coupled with the kinematic condition (2), i.e.

$$\partial_t h_0 + \partial_x(h_0\,u_0) = 0, \tag{21}$$

gives a closed system for $u_0(x,t)$ and $h_0(x,t)$, which is called the *strong slip model* [12].

3 Experiments and comparison with numerical results

In order to test the theoretical strong slip model we performed dewetting experiments with thin films of short-chained polystyrene (PS) on top of hydrophobized silicon wafers. We achieved 130 nm thick films of atactic PS (molecular weight 13.7 kg/mol, $M_w/M_n = 1.03$, PSS Mainz, Germany) by spincoating a toluene solution on mica, floating the films on fresh Millipore^{TM} water and

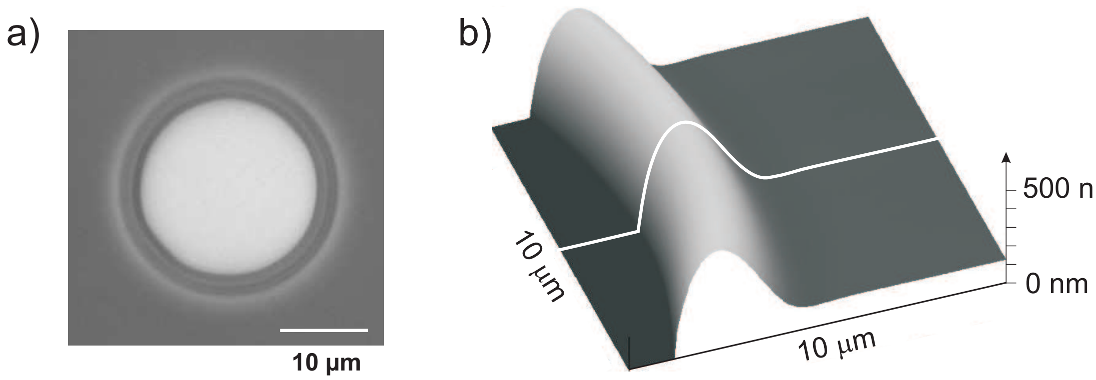

Figure 1: a) Optical image of a hole in a 130 nm thick PS(13.7k) film, dewetted from OTS on Si at 120 °C. b) AFM image of a section of the rim around the hole shown in a). A cross-section taken in radial direction (indicated by the white line) gives the rim profile which will be compared to the theory.

transferring them onto the coated wafers. To hydrophobize the substrates, we coated silicon wafers (2.1 nm native oxide layer, Wacker, Burghausen, Germany) with two different silane monolayers, octadecyltrichlorosilane (OTS) and the shorter dodecyltrichlorosilane (DTS) using standard techniques [16]. The rms roughness of both types of substrate as measured by atomic force microscopy (AFM) at $(1\,\mu\mathrm{m})^2$ scan size is below 0.15 nm. The contact angle of polystyrene droplets is $67(3)^\circ$ on both coatings, as AFM scans revealed.

In order to mobilize the films which are glassy at room temperature, we heated the samples to different temperatures (105 °C to 130 °C) above the glass transition of PS(13.7k), $T_g = 97\,°\mathrm{C}$. The dewetting process sets in by nucleation of holes which instantaneously start to grow [15, 17, 18]. Since we will only analyze the shape of the dewetting rim around the hole, the actual nucleation mechanism (homogeneous or heterogeneous) is irrelevant here. We observed the growth of holes by optical microscopy in order to determine the dewetting velocity. Once the holes had a radius of 12 μm, we rapidly quenched the samples to room temperature and measured the profiles of the holes with an atomic force microscope (AFM). See Fig. 1 for a typical image.

Comparing the profiles for PS films on OTS and DTS covered wafers at identical temperature, we find substantial differences, as shown in Fig. 2a) for 120 °C. Films on DTS exhibit a rim profile that decays monotonically towards the undisturbed film, whereas a film on the OTS layer exhibits an oscillatory decaying rim shape. To clarify the different rim morphologies, the inset to Fig. 2a) depicts $|H(X) - \bar{H}\,|$ in a semi-logarithmic plot. Here, $\bar{H}$ denotes the prepared film thickness.

In Fig. 2b) rim profiles calculated by the lubrication model (20) and (21) are shown for different slip lengths. For details of the simulations we refer to Refs. [12, 19]. Increasing the slip length b, we can observe a transition from oscillatory to monotonically decaying rim profiles.

In order to understand this morphological transition of rim shapes observed

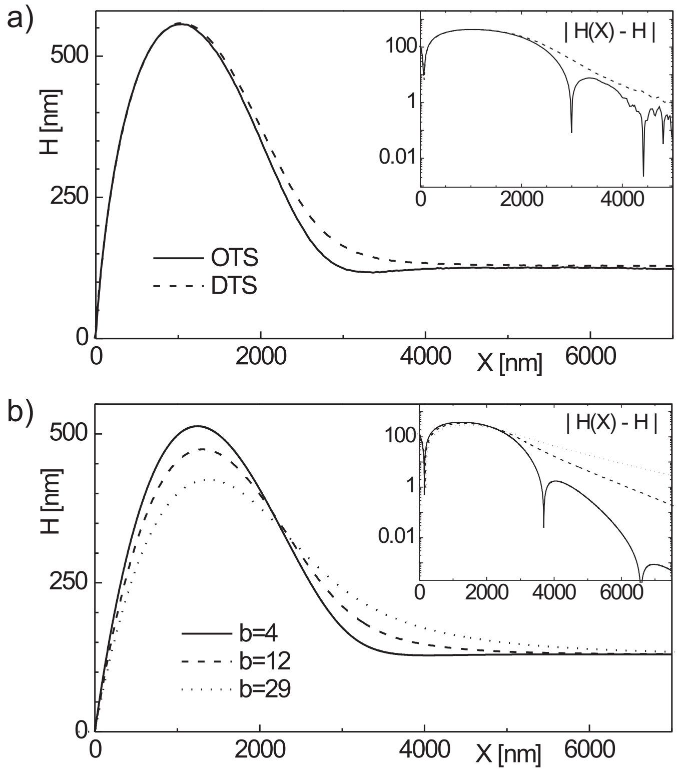

Figure 2: a) Rim profiles of holes of radius 12 μm in 130 nm thick PS(13.7k) films, dewetted at 120 °C. Depending on the substrate, OTS or DTS covered Si wafers, the profiles show a oscillatory or monotonically decaying rim towards the undisturbed film. b) Rim profiles calculated from the lubrication model for different slip lengths b nondimensionalized with $\bar{H} = 130$ nm.

in both the experiments and the simulations, we concentrate in the next section on the region where the rim connects to the undisturbed film and develop theoretical models to describe rim profiles.

4 Linear stability analysis about the undisturbed uniform film

The structure of the dewetting rim as it propagates into the undisturbed film can be found via linearized analysis. Note that for later comparison with experiments, the contribution from the intermolecular potential can be neglected. In the following, we analyze the shape of the rim close to the resting film. There, the film thickness is still close to the thickness of the flat resting film, which will be the base state. We linearize about this base state with respect to infinitesimal perturbations of the film thickness, flow velocity, etc., of size δ and obtain the shape of the leading edge of the rim.

4.1 Lubrication model

The base state of the strong slip model in Eqs. (20) and (21) is $h(x,t) = 1$ and $u(x,t) = 0$ about which we linearize with respect to infinitesimal perturbations of size δ,

$$h(x,t) \sim 1 + \delta\, \tilde{h}(x,t), \qquad u(x,t) \sim \delta\, \tilde{u}(x,t), \qquad \delta \ll 1, \tag{22}$$

and obtain the linearized equations

$$\begin{aligned} 4\,\partial_x^2 \tilde{u} + \partial_x^3 \tilde{h} - \frac{1}{\beta}\,\tilde{u} &= 0, && (23)\\ \partial_t \tilde{h} + \partial_x \tilde{u} &= 0. && (24) \end{aligned}$$

To describe the advancing edge of the ridge, it is convenient to shift into a frame of reference co-moving with the ridge, $\xi = x - s(t)$, and seek quasi-stationary solutions in the form of travelling fronts, $\tilde{h} = \tilde{h}(\xi)$. Then, the continuity equation (24) forces $\tilde{u} = \dot{s}\tilde{h}(\xi)$. Inserting this into the momentum equation (23) yields

$$4\,\dot{s}\,\partial_\xi^2 \tilde{h} + \partial_\xi^3 \tilde{h} - \frac{\dot{s}}{\beta}\,\tilde{h} = 0. \tag{25}$$

To understand the qualitative forms of the advancing ridge in this equation, we solve it with the ansatz $\tilde{h}(\xi) = \hat{h}\,\exp(\gamma\,\xi)$, yielding the characteristic equation

$$\chi_{\mathrm{lub}}(\gamma; \beta, \dot{s}) = \gamma^3 + 4\,\dot{s}\,\gamma^2 - \frac{\dot{s}}{\beta} = 0. \tag{26}$$

Note that in this equation γ depends on t parametrically through $s(t)$.

For the transitions in the ridge structure we note that Descartes' law of signs shows that there is one positive real root and either two negative or two complex conjugate roots. Physically relevant solutions, with $\tilde{h}(\xi \to \infty) \to 0$, must have $\Re(\gamma) < 0$. The change of roots from real to complex conjugate occurs when the discriminant vanishes, equivalently,

$$1 - \frac{256}{27}\,\beta\,\dot{s}^2 = 0. \tag{27}$$

From (27), we obtain an estimate for the critical ridge speed that separate real-decaying profiles (γ real) from oscillatory profiles (complex conjugate γ) in terms of the slippage

$$\dot{s}_{\rm crit} \sim \sqrt{\frac{3}{\beta}}\,\frac{3}{16}. \tag{28}$$

4.2 Stokes model

In order to show the range of validity and applicability of this result, it is instructive to go back to the full Stokes model. We start with equations (9)–(15), i.e., the Stokes model in the strong-slip scaling, but we keep all terms.

In two dimensions it is convenient to express the flow velocities in terms of the stream function

$$\partial_z \psi = u \quad \text{and} \quad -\partial_x \psi = w. \tag{29}$$

Then we can formulate the incompressible Stokes problem in Eqs. (9–11) coupled to the kinematic condition in Eq. (12) in terms of ψ and h. For the incompressible Stokes equations (9–11) we get

$$\partial_z^4 \psi + 2\,\varepsilon^2\,\partial_x^2 \partial_z^2 \psi + \varepsilon^4\,\partial_x^4 \psi = 0. \tag{30}$$

The boundary conditions at the film surface $z = h$ in Eqs. (12–14) become

$$\begin{aligned}
\partial_t h + \frac{d}{dx}\psi(x,h,t) &= 0, &(31)\\
\left(\partial_z^2 \psi - \varepsilon^2\,\partial_x^2 \psi\right)\left(1 - \varepsilon^2\,(\partial_x h)^2\right) - 4\,\varepsilon^2\,\partial_x h\,\partial_x \partial_z \psi &= 0, &(32)\\
\varepsilon^2\,\partial_x^2 \partial_z \psi + \partial_z^3 \psi - \left(\varepsilon^4\,\partial_x^3 \psi + \varepsilon^2\,\partial_x \partial_z^2 \psi\right)\,\partial_x h + \varepsilon^2\,\frac{d}{dx}\frac{\partial_x^2 h}{\left(1 + \varepsilon^2\,(\partial_x h)^2\right)^{3/2}} &\\
-2\,\varepsilon^2\,\frac{d}{dx}\frac{-\left(1 - \varepsilon^2\,(\partial_x h)^2\right)\,\partial_x \partial_z \psi - \partial_x h\,\left(\partial_z^2 \psi - \varepsilon^2\,\partial_x^2 \psi\right)}{1 + \varepsilon^2\,(\partial_x h)^2} &= 0, &(33)
\end{aligned}$$

respectively. Note that in order to be able to express the pressure in terms of ψ via Eqs. (9) and (10), Eq. (33) is the total derivative of Eq. (14) with respect to x. At $z = 0$ we get from Eq. (15)

$$\psi = 0 \quad \text{and} \quad \partial_z \psi - b\,\partial_z^2 \psi = 0. \tag{34}$$

As in the previous section we now linearize about the undisturbed base state $h = 1$ and $\psi = 0$, i.e., about the flat and resting film, by perturbing via

$$h = 1 + \delta\,\tilde{h} \quad \text{and} \quad \psi = \delta\,\tilde{\psi}, \tag{35}$$

with $\delta \ll 1$. We then transform to the moving frame coordinate $\xi = x - s(t)$ and make the ansatz

$$\tilde{\psi}(x,z,t) = \hat{\psi}(z)\, \exp(\gamma\,\xi) \quad \text{and} \quad \tilde{h}(x,t) = \hat{h}\, \exp(\gamma\,\xi) \tag{36}$$

Keeping only the $O(\delta)$ terms we obtain the linearized problem for the full Stokes model in Eq. (30)

$$\partial_z^4\hat{\psi} + 2\,(\varepsilon\,\gamma)^2\partial_z^2\hat{\psi} + (\varepsilon\,\gamma)^4\hat{\psi} = 0 \tag{37}$$

in $0 < z < 1$, with boundary conditions at the film surface at $z = 1$ (corresponding to Eqs. (32) and (33))

$$(\varepsilon\,\gamma)^2\hat{\psi} - \partial_z^2\hat{\psi} = 0 \tag{38}$$

$$3\,(\varepsilon\,\gamma)^2\partial_z\hat{\psi} + \frac{(\varepsilon\,\gamma)^3}{\varepsilon\,\dot{s}}\,\hat{\psi} + \partial_z^3\hat{\psi} = 0, \tag{39}$$

and at the substrate surface at $z = 0$ (derived from Eq. (34))

$$\hat{\psi} = 0 \quad \text{and} \quad \partial_z\hat{\psi} - b\,\partial_z^2\hat{\psi} = 0. \tag{40}$$

The general solution for the linear ordinary differential equation in Eq. (37) is

$$\hat{\psi}(z) = c_1\, e^{i\,\varepsilon\,\gamma\,z} + c_2\, e^{-i\,\varepsilon\,\gamma\,z} + c_3\, z\, e^{i\,\varepsilon\,\gamma\,z} + c_4\, z\, e^{-i\,\varepsilon\,\gamma\,z}. \tag{41}$$

Inserting this into the boundary conditions (38)–(40) yields a system of linear homogeneous equations for the coefficients $c_1, \ldots, c_4$. This system has a non-trivial solution, indicating an eigensolution of (37)–(40), if the determinant of this system is zero. The determinant one easily finds to be (after multiplication with $\dot{s}\,b\,(\varepsilon\,\gamma)^4/16$)

$$\begin{aligned}\chi_\mathrm{S}(\gamma; b, \dot{s}) = &\left(-\varepsilon^2\,\dot{s}\,\gamma + \frac{1}{4\,b}\right)\,\sin(2\,\varepsilon\,\gamma) + \left(\frac{\varepsilon\,\dot{s}}{2\,b} + \frac{\varepsilon\,\gamma}{2}\right)\,\cos(2\,\varepsilon\,\gamma)\\ &- 2\,\left(1 + \frac{1}{2\,b}\right)\,\varepsilon\,\dot{s}\,(\varepsilon\,\gamma)^2 - \left(\frac{1}{2} + \frac{1}{2\,b}\right)\,\varepsilon\,\gamma + \frac{\varepsilon\,\dot{s}}{2\,b}.\end{aligned} \tag{42}$$

For (42), we seek the solutions γ which have a negative real part, since we require that the perturbed profile $\tilde{h}(x,t) \to 1$ as $x \to \infty$. Furthermore, we focus on the case where the decay is consistent with the basic assumption of lubrication theory, namely, that the length scale ratio, measured for example by the typical spatial derivative of the unscaled film thickness, is of order ϵ. For the scale variable $\tilde{h}(x,t)$ given in (36), this can be satisfied by requiring that $\tilde{h}_x/h = \gamma$ is of order one.

Thus, $\epsilon\gamma$ is assumed to be small and we can approximate χ_S by its Taylor expansion for $\epsilon\gamma \ll 1$.

$$\chi_\mathrm{T}(\gamma; b, \dot{s}) = \left(1 + \frac{1}{3b}\right)(\varepsilon\gamma)^3 + 4\varepsilon\dot{s}\left(1 + \frac{1}{2b}\right)(\varepsilon\gamma)^2 - \frac{\varepsilon\dot{s}}{b} = 0. \tag{43}$$

If we now recall $b = \beta/\varepsilon^2$ for the strong slip regime, and take the limit $\varepsilon \to 0$ keeping $\beta = O(1)$ fixed, we obtain to leading order the characteristic equation $\chi_\mathrm{lub}(\gamma; \beta, \dot{s})$ for the strong-slip lubrication model, i.e., equation (26).

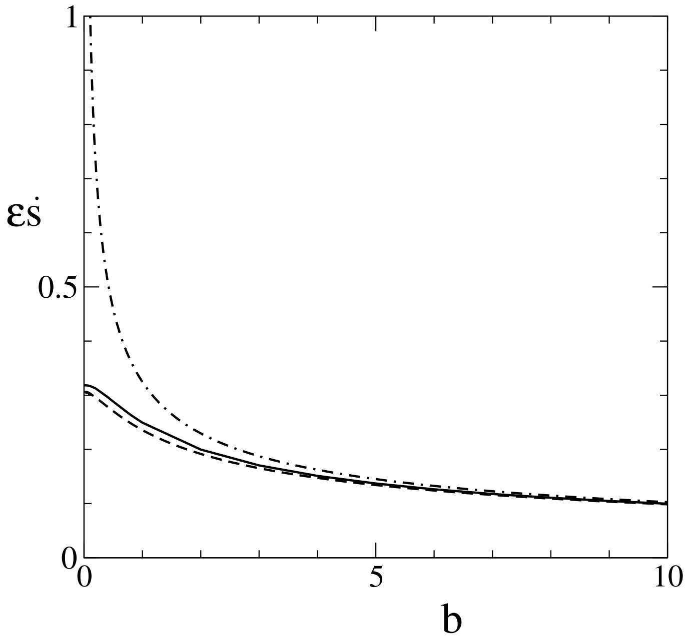

Figure 3: Comparison of the critical $\dot{s}(b)$, given by (45), at which the dominant eigenvalues γ that govern the spatial decay of the film profile change from complex conjugate (for $\dot{s} < \dot{s}_{crit}(b)$) to two real eigenvalues (for $\dot{s} > \dot{s}_{crit}(b)$). The solid, dashed, and dash-dotted lines are, respectively, the critical $\dot{s}_{crit}(b)$ for the eigenvalues obtained from for full Stokes model, $\chi = \chi_{\rm S}$, for third order Taylor approximation of $\chi_{\rm S}$, i.e, $\chi = \chi_{\rm T}$, and for the strong slip lubrication model, where $\chi = \chi_{\rm lub}$.

Before proceeding, let us note that rescaling the dewetting speed as $\dot{s} = \varepsilon^2 \dot{s}^*$, taking the limit $\varepsilon \to 0$ keeping $\dot{s}^* = O(1)$ and $b = O(1)$ fixed (in contrast to the scaling $b = \beta/\varepsilon^2$ with $\beta = O(1)$ in the rest of the paper), one finds to leading order in ε the characteristic equation for the weak-slip regime

$$\chi_{\rm weak}(\gamma; b, \dot{s}^*) = \gamma^3 - \frac{\dot{s}^*}{b + 1/3} = 0. \tag{44}$$

Next, we focus on the two dominant decaying modes γ_1 and γ_2 for the spatial decay of the film profile, for each of the three characteristic equations, i.e., $\chi_{\rm lub}$, $\chi_{\rm S}$, and $\chi_{\rm T}$. These modes are given by $\chi = 0$ with $\mathrm{Re}(\gamma) < 0$ for which the modulus of is smallest. They can be either two real negative or a complex conjugate pair of values. Note that $\chi_{\rm T}$ and $\chi_{\rm lub}$ are cubic polynomials with at most three zeros, while $\chi_{\rm S}$ is a transcendental equation which can have infinitely many solutions for $\chi_{\rm S} = 0$.

Inspection of these two dominant modes shows that for each of the three χ's, the eigenvalues are complex conjugate for $(b, \dot{s})$ below a certain line, and real above it. The line is characterized by a merging of the two values to one real double root of the equation, i.e., for those $(b, \dot{s}(b))$ that satisfy

$$\chi(\gamma; b, \dot{s}) = 0 \qquad \text{and} \qquad \frac{d}{d\gamma}\chi(\gamma; b, \dot{s}) = 0. \tag{45}$$

For χ_{S}, these equations have to be solved numerically to obtain $\varepsilon\dot{s}^{S}_{\mathrm{crit}}(b)$, while for χ_{T} and χ_{lub} we obtain

$$\varepsilon\dot{s}^{T}_{\mathrm{crit}} = \frac{3\sqrt{3}}{16}\frac{b+1/3}{(b+1/2)^{3/2}}, \tag{46}$$

$$\varepsilon\dot{s}^{lub}_{\mathrm{crit}} = \frac{3\sqrt{3}}{16}b^{-1/2}, \tag{47}$$

respectively. The comparison is done in Fig. 3 and shows that the result for $\varepsilon\dot{s}^{T}_{\mathrm{crit}}$ yields a good approximation for the curve $\varepsilon\dot{s}^{S}_{\mathrm{crit}}(b)$ of the full model for all values of b, while the approximation quality of the value $\varepsilon\dot{s}^{lub}_{\mathrm{crit}}$ obtained from strong slip lubrication model deteriorates for small b as expected.

5 Method to quantify slippage and its validity

5.1 Method

The process of determining the slip length from the shape of a moving rim essentially reverses the above considerations: from the experimentally measured rim shape the two dominant decaying spatial modes γ_1 and γ_2 are extracted. Using these values, the slip length B as well as the capillary number Ca can be determined from the characteristic equation $\chi = 0$. Since the full Stokes model χ_{S} ends up in quite cumbersome expressions for B and Ca, we focus in the following section on the strong slip lubrication model.

To get the values for γ_1 and γ_2 (or rather their dimensional form $\Gamma_{1/2} = \gamma_{1/2}/\bar{L}$) from the experimentally observed rim profiles, one has to fit the respective function $H(\Xi) = \bar{H} + \delta\tilde{H}(\Xi)$ to the data in the region of small perturbation of the undisturbed film of thickness $\bar{H}$. Note that $\Xi = \bar{L}\,\xi$ denotes the dimensional form of the abscissa ξ. For the fitting procedure, we used data points of the profiles up to a maximal height of about 120% of $\bar{H}$. In the case of oscillatory decaying profiles (i.e., when a local minimum of the film height exhibits where the rim is connected to the undisturbed film, eventually followed by a local maximum), Γ_1 and Γ_2 are a pair of two complex conjugate numbers $\Gamma_{1/2} = \Gamma_r \pm i\,\Gamma_i$ with negative Γ_r. Here, an exponentially damped oscillation $\delta\tilde{H}_{osci} = \delta\tilde{H}_0\,\exp(\Gamma_r\,\Xi)\,\cos(\Gamma_i\,\Xi + \phi)$ (fit parameters are $\delta\tilde{H}_0$, Γ_i, Γ_r, and ϕ) captures the decay towards the resting film thickness $\bar{H}$ in the experimental data very well, cf. Fig. 4. From the fit we gain the inverse decay length Γ_r and the wave number Γ_i, and thus $\Gamma_{1/2} = \Gamma_r \pm i\,\Gamma_i$. In the case of monotonically decaying rims, the data can be fitted by a superposition of two exponentials $\delta\tilde{H}_{mono} = \delta\tilde{H}_1\,\exp(\Gamma_1\,\Xi) + \delta\tilde{H}_2\,\exp(\Gamma_2\,\Xi)$ (fit parameters $\delta\tilde{H}_{1/2}$ and $\Gamma_{1/2}$) with the inverse decay lengths Γ_1 and Γ_2.

Knowing Γ_1 and Γ_2, these values can now be used to determine the slip length and the capillary number of the investigated system. For this purpose, we recall the characteristic equation of the strong slip lubrication model in dimensional form

$$\chi_{\mathrm{lub}}(\Gamma; B, \mathrm{Ca}) = (\bar{H}\,\Gamma)^3 + 4\,\mathrm{Ca}\,(\bar{H}\,\Gamma)^2 - \mathrm{Ca}\,\frac{\bar{H}}{B} = 0, \tag{48}$$

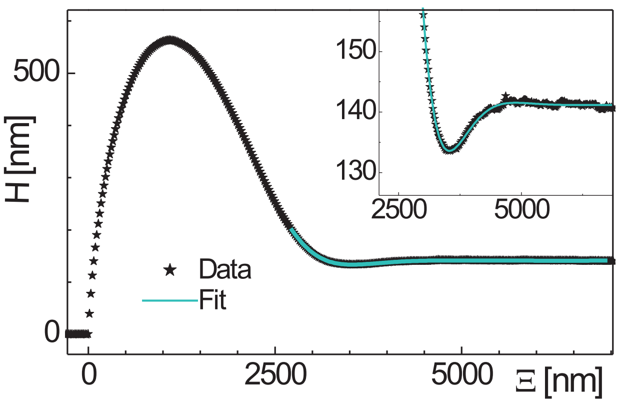

Figure 4: The profile of the rim shown in Fig. 1 is in the region where it decays towards the undisturbed film, ie., for small perturbation, well fitted by an exponentially decaying oscillation.

where the capillary number is $\mathrm{Ca} = \eta\,\dot{S}/\sigma$ with the characteristic speed of the rim $\dot{S} = \bar{U}\,\dot{s}$. Knowing two roots Γ_1 and Γ_2 of Eq. (48) we get two equations with the two unknowns B and Ca for which we can solve and get

$$B_{lub} = \frac{1}{4\bar{H}} \frac{\Gamma_1^2 + \Gamma_1\Gamma_2 + \Gamma_2^2}{\Gamma_1^2\Gamma_2^2}, \qquad \mathrm{Ca}_{lub} = -\frac{\bar{H}}{4} \frac{\Gamma_1^2 + \Gamma_1\Gamma_2 + \Gamma_2^2}{\Gamma_1 + \Gamma_2}. \tag{49}$$

Additionally, the film viscosity η can be determined from the capillary number Ca, using the surface tension $\sigma = 30.8$ mN/m and the observed dewetting velocity $\dot{S}$. We like to emphasize that in order to determine solely the slip length, the knowledge of neither the dewetting velocity nor the viscosity is required.

In order to check the consistency of the above explained analysis we performed a couple of tests with the experimental data. Firstly, we determined the viscosity from the extracted capillary number from profiles on OTS and DTS at different temperatures. The viscosity was found to be in line with rheometric data, cf. Fig. 5. A second test was the variation of the film thickness which leads to different values for $\Gamma_{1/2}$ and $\dot{S}$ but which does not change the slip length and the viscosity. Indeed, the extracted slip length was independent of initial film thickness. In a third and last consistency check we analyzed holes of various sizes. With growing hole diameter the rim gets larger. Since friction forces increase with rim size, the dewetting velocity slows down. As a consequence, a more pronounced oscillatory shape can be found, resulting in a variation of the fitting parameters Γ_1 and Γ_2 with hole size. However, the slip lengths and viscosities obtained via Eq. (49) were independent of the hole size as expected. For details we refer to Ref. [13].

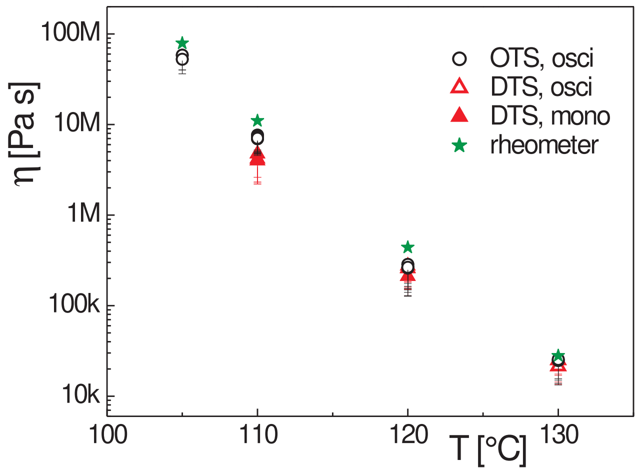

Figure 5: Viscosity as a function of temperature. The results of rim shape analysis of PS films on OTS and DTS are compared with viscosity data from independent rheometric measurements; 'osci' and 'mono' indicate the used fitting functions $\delta\tilde{H}_{osci}$ and $\delta\tilde{H}_{mono}$, respectively.

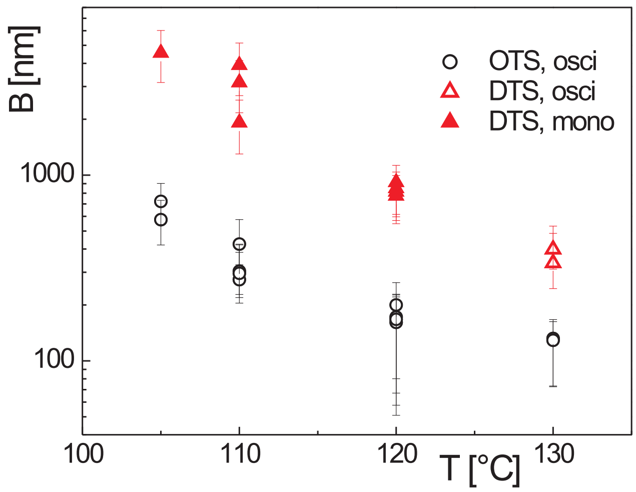

Figure 6: Slip length B for PS(13.7k) on OTS and DTS coatings as a function of melt temperature. The data are extracted from rim profiles of holes of radius 12 μm in 130 nm thick films.

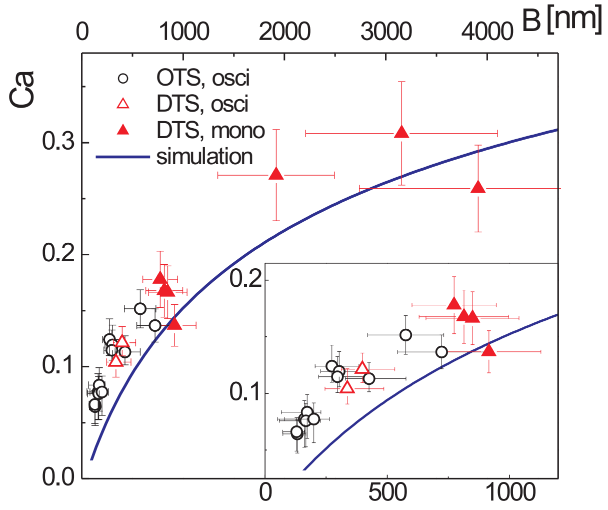

Figure 7: Capillary number Ca extracted from the rims analyzed in Fig. 6. Plotting Ca versus the respective slip lengths, the data collapses on one curve. The solid line indicates the result of simulations. The inset depicts a zoom to the region of slip lengths below 1 μm.

5.2 Results and discussion

Since all tests show consistent results for both the viscosity and the slip length, we can rely on the analysis method. In Fig. 6 the results for polystyrene films of constant molecular weight (13.7 kg/mol) and constant initial film thickness (130 nm) are summarized. All data shown here are extracted from rims of the same volume. We find that the amount of slippage depends on both the substrate underneath and the melt temperature. For polystyrene films on the DTS coating, the slip length is about one order of magnitude larger than on OTS. On both coatings, however, slippage decreases for increasing melt temperature.

Plotting the capillary number obtained by rim shape analysis versus the slip length, as shown in Fig. 7, we find that the data from different substrates collapses on one curve. By varying the dewetting temperature or the type of substrate underneath, we can change the amount of slippage and hence probe this curve successively. As expected, the dewetting velocity $\dot{S}$ and with it the capillary number $\mathrm{Ca} = \eta\,\dot{S}/\sigma$ increases for increasing slip length. But this behavior is found to be clearly non-linear.

From the simulations shown in Fig. 2b, which were based on the lubrication model in Eqs. (20) and (21), we can in addition to the rim profile calculate the dewetting velocity $\dot{S}$ at the stage when the rim size matches the one of the experiments. Doing this for different numbers of the slip length, we gain the capillary number as function of B. This curve is shown in Fig. 7 as the solid line. The qualitative behavior is in good agreement to the experimental data. However, a shift to lower capillary numbers can be observed. This may have various reasons. Firstly, the calculation was done for straight fronts, whereas in the experiments the growth of circular holes is investigated. For the analyzed experiments with hole radii 12 μm, however, the curvature of the contact line is negligible compared to the curvature of the rim in radial direction. Secondly, in the simulations only linear curvatures were taken into account.

Results for the weak slip model with linearized curvature and with nonlinear curvature in the expression for the surface tension suggest that the former tend to underestimate the dewetting rate [20, 19]. This is consistent with the observation that higher contact angles are typically associated with higher dewetting rates [19, 21, 17, 22], and inclusion of nonlinear curvature generally leads to higher contact angles: The static contact angle θ_S for the nonlinear curvature case is given by

$$1 - (1 + \tan^2 \theta_S)^{-1/2} = -\frac{1}{\sigma} \min_h \phi(h),$$

or

$$1 - \cos \theta_S = -\frac{1}{\sigma} \min_h \phi(h), \tag{50}$$

see for example [15], and from this we obtain for the linearized curvature case ($\tan \theta_S \ll 1$):

$$\frac{1}{2} \tan^2 \theta_S = -\frac{1}{\sigma} \min_h \phi(h). \tag{51}$$

One easily finds that for $0 \leq \theta_S \leq \pi/2$, the expression (51) results in larger contact angles than (50). Note also the steeper fronts in the dewetting profiles for the nonlinear curvature models in [20]. All these facts may explain the shift in capillary number shown in Fig. 7.

Let us for a moment focus on a special region in the Ca(B) plot. There is a specific regime near the transition from oscillatory to monotonic rims where the fitting procedure is not straight forward. Note that the 'monotonic' fitting function $\delta\tilde{H}_{mono} = \delta\tilde{H}_1 \exp(\Gamma_1 \Xi) + \delta\tilde{H}_2 \exp(\Gamma_2 \Xi)$, which is the solution for real Γ_1 and Γ_2, exhibits a local minimum and approximates zero from negative values, if one of the coefficients $\delta\tilde{H}_1$ or $\delta\tilde{H}_2$ is negative. Hence, for profiles showing a local minimum between the rim and the undisturbed film but which do not show a clearly pronounced second maximum, both functions $\delta\tilde{H}_{osci}$ and $\delta\tilde{H}_{mono}$ may capture the data. We have fitted both functions to a number of profiles in that regime and extracted the slip lengths as well as the respective capillary numbers. The results for B shown in Fig. 8 correspond to a growing hole in a 130 nm thick PS film dewetting from OTS at 110 °C as captured by in situ AFM. For small holes, the function $\delta\tilde{H}_{mono}$ captures the monotonic profiles very well, and the results for the slip length are reasonable. For radii between about 1.5 and 5 μm the rim profile exhibits a local minimum. The function $\delta\tilde{H}_{mono}$ still captures the rim shapes when choosing one negative coefficient $\delta\tilde{H}_{1/2}$, however, the extracted slip lengths are not independent of R. The identical rim profiles fitted by $\delta\tilde{H}_{osci}$ result in a constant slip length. For holes of radii larger than 5 μm the function $\delta\tilde{H}_{mono}$ does not capture the oscillatory rim profiles at all. The described consistency check for various rim sizes provides a general argument that excludes the case of negative coefficients $\delta\tilde{H}_{1/2}$ in the fitting function $\delta\tilde{H}_{mono}$ for real $\Gamma_{1/2}$.

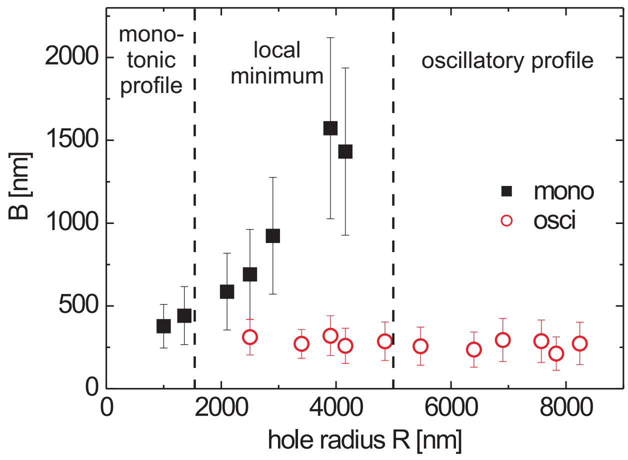

Figure 8: Near the transition between monotonically and oscillatorily decaying rims, profiles with a clear minimum can be fitted by both functions $\delta\tilde{H}_{mono}$ or $\delta\tilde{H}_{osci}$. Using the function for real $\Gamma_{1/2}$, $\delta\tilde{H}_{mono}$, the results for B are much larger than for fitting the profiles by $\delta\tilde{H}_{osci}$. The data correspond to a 130 nm thick PS(13.7k) film dewetting from OTS at 110 °C, as captured by in situ AFM.

5.3 Limitation of validity

For the rim analysis as described above we need two inverse decay lengths Γ_1 or Γ_2. However, in the case of extremely large slip lengths and asymmetric rims, the second inverse decay length is to large to be observed experimentally. As a consequence, it is not possible to determine neither the capillary number nor the slip length solely from the rim profile. However, if the capillary number is measured independently, one of the inverse decay lengths is sufficient to determine the slip length. In our experiments, the described situation occurs for 130 nm thick PS(13.7k) films on the DTS coating, dewetting at 105 °C. By using independently measured viscosity and velocity data, the capillary number can be determined. From the fit to the rim profile we have Γ_1. Inserting now Ca and Γ_1 in the characteristic equation (48), the slip length in this situation is found to be about 5 μm, which corresponds to the ratio $b = B/\bar{H} \approx 40$. The same experiment at 110 °C exhibits a slip length of about 3 μm, hence $b \approx 20$. This turns out to be about the limit up to which both inverse decay lengths Γ_1 and Γ_2 can be extracted from the measured rim profile. For polystyrene films of higher molecular weight (above 100 kg/mol), the rim gets more and more asymmetric [23], indicating an increasing slip length. Hence, in most cases the slip length is expected to exceed the upper limit of $b \approx 20$.

In the examples described above, we used the strong slip model in order to extract the capillary number and the slip length out of the rim profiles. However, this model is only valid for slip lengths larger than the film thickness. The smallest B observed in our experiments for PS(13.7) films on OTS at 130 °C was in the order of $\bar{H}$. For systems with much smaller slip lengths

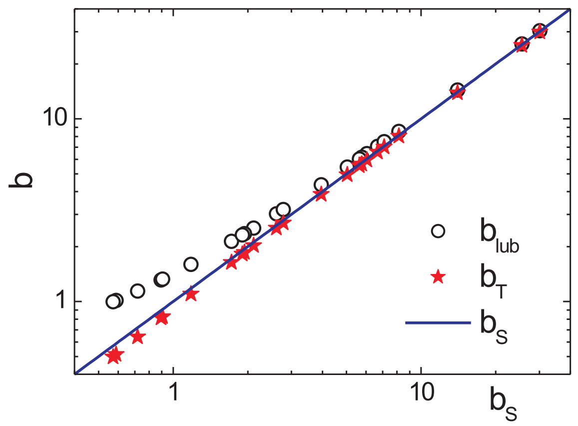

Figure 9: Comparison of slip parameters that yield the same two (real or complex) spatially decaying modes using either the strong slip model $\chi_{\rm lub}$ (open circles), the third Taylor expansion of the Stokes model $\chi_{\rm T}$ (stars), or the full Stokes model $\chi_{\rm S}$ (solid line). The data correspond to the rim profiles analyzed in Fig. 6.

the strong slip model will produce systematic errors. As shown in Fig. 3, the critical dewetting velocity $\dot{s}_{crit}(b)$ as obtained from the strong slip model deviates from the actual value obtained from the full Stokes model significantly for small b.

The validity and accuracy of the strong slip lubrication approximation can be assessed by comparison with the result for the full Stokes model. Fig. 9 shows slip parameters determined by the lubrication model $\chi_{\rm lub}$, $b_{lub} = B_{lub}/\bar{H}$, in comparison to results using the Stokes model $\chi_{\rm S}$, $b_S = B_S/\bar{H}$. There are quite strong deviations for weak slippage, i.e., for $b < 1$. For rim shape analysis in practise, however, it is not convenient to use the full Stokes model $\chi_{\rm S}$, since the expressions for B_S and ${\rm Ca}_S$ are rather longish and cumbersome. So we use the (apparently quite accurate) Taylor approximation instead. The respective characteristic equation (43) in dimensional form is given by

$$\chi_{\rm T}(\Gamma; B, {\rm Ca}) = \left(1 + \frac{\bar{H}}{3B}\right)(\bar{H}\,\Gamma)^3 + 4{\rm Ca}\left(1 + \frac{\bar{H}}{2B}\right)(\bar{H}\,\Gamma)^2 - {\rm Ca}\frac{\bar{H}}{B} = 0. \quad (52)$$

Knowing two roots Γ_1 and Γ_2 of Eq. (52) from rim shape analysis, we get two equations with the two unknowns B and Ca for which we can solve and obtain

$$B_T = \frac{1}{4\bar{H}}\frac{\Gamma_1^2 + \Gamma_1\Gamma_2 + \Gamma_2^2}{\Gamma_1^2\Gamma_2^2} - \frac{\bar{H}}{2}, \qquad {\rm Ca}_T = \frac{\bar{H}^{\,3}}{6}\frac{\Gamma_1^2\Gamma_2^2}{\Gamma_1 + \Gamma_2} - \frac{\bar{H}}{4}\frac{\Gamma_1^2 + \Gamma_1\Gamma_2 + \Gamma_2^2}{\Gamma_1 + \Gamma_2}. \quad (53)$$

Note that the expression for B_T in (53) differs from the lubrication result B_{lub} in (49) by exactly $\bar{H}/2$. Note also that Eq. (52) is also valid for small values of B, i.e., for the regime in which one would use the weak slip lubrication model which leads to Eq. (44). However, using the characteristic equation (44) one cannot determine both Ca and B from the rim shape.

The results for $b_T = B_T/\bar{H}$ are shown in Fig. 9 in comparison to the values b_{lub} and b_S. Using the strong slip lubrication model χ_{lub} instead of the full Stokes model χ_{S}, the relative error for the extracted slip length increases significantly for decreasing slippage. However, when using χ_{T}, the deviation of the calculated slip length is quite small, even for weak slippage. Since no limitation for small slip lengths is given for the third Taylor expansion of the full Stokes model, the respective Eq. (53) is recommended to be used for the determination of slippage by rim shape analysis.

6 Conclusions and outlook

In this article, we have shown both experimentally and theoretically that slippage significantly affects the rim shape of dewetting thin liquid films: slowly moving fronts with no or weak slip at the solid/liquid interface develop an oscillatory decaying rim - i.e., complex eigenvalues of the characteristic equation χ of linear stability analysis in a co-moving frame - whereas strong slippage and faster dewetting result in a monotonically decaying shape, corresponding to real negative roots of χ. The critical line between complex and real solutions, i.e., where this morphological transition of the rim shape occurs, could be very accurately predicted by a new model applied: instead of using a lubrication model χ_{lub} that only accounts for large slip lengths, we calculated the third order Taylor expansion χ_{T} of the characteristic equation obtained from the full Stokes model, χ_{S}. The analytical solution for the transition line using χ_{T} compares very well to the numerical solution obtained from the Stokes model, even for weak slippage.

Moreover, we developed a method for extracting the slip lengths of dewetting liquid films using rim shape analysis. For short-chained polystyrene films on the DTS coating we found slip lengths about one order of magnitude larger than for the same films on OTS. Additionally, on both coatings, the slip length decreases for increasing melt temperature. As already seen for the critical line of morphology transition, the results for the slip length gained from the lubrication model χ_{lub} are a rather good approximation in the regime of strong slippage. More accurate results for the whole range of slip lengths, however, can be obtained by using χ_{T}, the third order Taylor expansion of the full Stokes model.

7 Acknowledgments

The authors thank O. Bäumchen for helpful discussions. This work was supported in part by the Heisenberg-scholarship DFG Grant MU 1626/3 (AM), the DFG Research Center Matheon Berlin (AM and BW), the DFG Grants MU 1626/5 (AM and BW), RA 1061/2 (MR), and Ja 905/3 (KJ) within the priority program SPP 1164, and the European Graduate School GRK 532 (RF). RF and KJ acknowledge generous support of Si wafers by Siltronic AG,

Burghausen, Germany.

References

[1] Tretheway, D. C.; Meinhart, C. D. *Phys. Fluids* **2002**, *14*, L9 and **2004**, *16*, 1509.

[2] Lumma, D.; Best, A.; Gansen, A.; Feuillebois, F.; Radler, J. O.; Vinogradova, O. I. *Phys. Rev. E* **2003**, *67*, 056313.

[3] Pit, R.; Hervet, H.; Léger, L. *Phys. Rev. Lett.* **2000**, *85*, 980.

[4] Schmatko, T.; Hervet, H.; Léger, L. *Phys. Rev. Lett.* **2005**, *94*, 244501.

[5] Craig, V. S. J.; Neto, C.; Williams, D. R. M. *Phys. Rev. Lett.* **2001**, *87*, 054504.

[6] Vinogradova, O. I.; Yakubov, G. E. *Langmuir* **2003**, *19*, 1227.

[7] Cottin-Bizonne, C.; Jurine, S.; Baudry, J.; Crassous, J.; Restagno, F.; Charlaix, E. *Eur. Phys. J. E* **2002**, *9*, 47.

[8] Zhu, Y.; Granick, S. *Langmuir* **2002**, *18*, 10058.

[9] Lauga, E.; Brenner, M.; Stone, H. A. In *Handbook of Experimental Fluid Dynamics*; Foss, J., Tropea, C., Yarin, A., Eds.; Springer: New-York (2005); cond-mat/0501557.

[10] Neto, C.; Evans, D. R.; Bonaccurso, E.; Butt, H.-J.; Craig, V. S. J. *Rep. Prog. Phys.* **2005**, *68*, 2859.

[11] Fetzer, R.; Jacobs, K.; Münch, A.; Wagner, B.; Witelski, T. P. *Phys. Rev. Lett.* **2005**, *95*, 127801.

[12] Münch, A.; Wagner, B.; Witelski, T. P. *J. Engr. Math.* **2005**, *53*, 359.

[13] Fetzer, R.; Rauscher, M.; Münch, A.; Wagner, B. A.; Jacobs, K. *Europhys. Lett.* **2006**, *75*, 638.

[14] Evans, P. L.; King, J. R.; Münch, A. *AMRX Applied Mathematics Research eXpress* **2006**, *2006*, 25262.

[15] Seemann, R.; Herminghaus, S.; Jacobs, K. *Phys. Rev. Lett.* **2001**, *86*, 5534.

[16] Wassermann, S. R.; Tao, Y.-T.; Whitesides, G. M. *Langmuir* **1989**, *5*, 1074.

[17] Redon, C.; Brochard-Wyart, F.; Rondelez, F. *Phys. Rev. Lett.* **1991**, *66*, 715.

[18] Reiter, G. *Phys. Rev. Lett.* **2001**, *87*, 186101.

[19] Münch, A. *Journal of Physics: Condensed Matter* **2005**, *17*, S309.

[20] Münch, A.; Wagner, B. *Physica D* **2005**, *209*, 178.

[21] Reiter, G.; Khanna, R. *Langmuir* **2000**, *16*, 6351.

[22] Flitton, J. C.; King, J. R. *J. Engrg. Math.* **2004**, *50*, 241.

[23] Seemann, R.; Herminghaus, S.; Jacobs, K. *Phys. Rev. Lett.* **2001**, *87*, 196101.